




Article

Anion-Dependent Cu(II) Coordination Polymers: Geometric, Magnetic and Luminescent Properties

Ihsan Ullah ¹, Jong Won Shin ¹, Ryuya Tokunaga ², Shinya Hayami ², Hye Jin Shin ³ and Kil Sik Min ^{3,*}¹ Department of Chemistry, Kyungpook National University, Daegu 41566, Korea² Department of Chemistry, Kumamoto National University, Kumamoto 860-8555, Japan³ Department of Chemistry Education, Kyungpook National University, Daegu 41566, Korea

* Correspondence: minks@knu.ac.kr; Tel.: +82-53-9505906; Fax: +82-53-9505899

Abstract: A one-dimensional (1D) coordination polymer [Cu₂(bpba)(CH₃COO)₄] (**1**) and a two-dimensional (2D) coordination polymer [Cu(bpba)₂(H₂O)(NO₃)](NO₃)·2H₂O·MeOH (**2**) were synthesized by the reaction between Cu(CH₃COO)₂·H₂O/Cu(NO₃)₂·3H₂O and bis(4-pyridyl)benzylamine (bpba). The Cu(II) ions of **1** and **2** have distorted-square pyramidal coordination with a paddle-wheel structure and an octahedral geometry, respectively. By coordinating the Cu(II) ions and bpba ligands, **1** and **2** formed zigzag 1D and puckered 2D coordination polymers, respectively. Polymer **1** exhibits strong emissions at 355 and 466 nm, whereas polymer **2** exhibits strong emissions only at 464 nm. The emissions are strongly dependent on the geometry of the Cu(II) ions linked by the bpba and anionic ligands. Polymer **1** exhibits a very strong antiferromagnetic interaction within the paddle-wheel dimer, whereas polymer **2** exhibits a very weak antiferromagnetic interaction through the bpba linkers and/or space.

Keywords: crystal engineering; coordination polymer; Cu(II) ion; photoluminescence; structure; magnetism



Citation: Ullah, I.; Shin, J.W.; Tokunaga, R.; Hayami, S.; Shin, H.J.; Min, K.S. Anion-Dependent Cu(II) Coordination Polymers: Geometric, Magnetic and Luminescent Properties. *Crystals* **2022**, *12*, 1096. <https://doi.org/10.3390/cryst12081096>

Academic Editor: Raghvendra Singh Yadav

Received: 12 July 2022

Accepted: 2 August 2022

Published: 5 August 2022

Publisher's Note: MDPI stays neutral with regard to jurisdictional claims in published maps and institutional affiliations.



Copyright: © 2022 by the authors. Licensee MDPI, Basel, Switzerland. This article is an open access article distributed under the terms and conditions of the Creative Commons Attribution (CC BY) license (<https://creativecommons.org/licenses/by/4.0/>).

1. Introduction

Metal-organic coordination polymers have attracted considerable attention because of their prominent functionalities, such as porosity, luminescence, and molecular magnetism [1–6].

These functional features are exploited by designing unique-network structures using metal ions, organic ligands, and counter anions [7]. In other words, various network structures can be constructed based on the choice and combination of components. For example, the Cu(II) ion, as a metal linker, is a d⁹ system and has a Jahn–Teller distortion effect [8]. These factors can influence the geometric structure and physical properties of Cu(II) complexes. That is, the elongated axial bonds in the Cu(II) coordination compounds can induce unique electronic effects, such as molecular catalysis and magnetism [9–11].

Acetate can form a paddle-wheel Cu(II) dimer unit [Cu₂(CH₃COO)₄], which is a good building block for molecule-based magnets and multidimensional coordination polymers [12–15]. In dimeric units, strong magnetic interactions are operative within the Cu₂ species, and the units form interesting coordination networks because of the vacant sites at the apical positions. Nitrate anions can generate more diverse structures owing to their weaker coordination ability than that of acetate [16–18].

Moreover, polydentate pyridine-based ligands have been used as linkers in Cu(II) coordination polymers [19,20]. These ligands can be connected to Cu(II) ions through pyridine groups and induce photoluminescence properties owing to the pyridine moieties. For example, Dang et al. reported a 2D layered-network structure including a tetra Cu(II) quadrangular unit [Cu^{II}₄(L₁)₄], exhibiting luminescence at 331 and 400 nm, originating from intra-ligand π–π* charge transfer (L₁ = N,N'-bis-(1-pyridin-4-yl-ethylidene)-hydrazine) [21]. Ding et al. reported a 2D Cu(II) coordination polymer {[Cu(μ₂-L₂)₂(NCS)₂]·0.5H₂O}_n with a

bidentate bridging L_2 ligand around the central Cu(II) ion ($L_2 = 3$ -(5-methyl-1,3,4-oxadiazol-2-yl)pyridine) [22]. The Cu(II) polymer exhibited antiferromagnetic interactions between the central Cu(II) ions without any luminescent emissions.

In this context, bidentate bis-(4-pyridyl) benzylamine (bpba) was used as a linker for the self-assembly of Cu(II) metal ions to obtain supramolecular frameworks. Thus, here, Cu(II) coordination polymers, $[\text{Cu}_2(\text{bpba})(\text{CH}_3\text{COO})_4]$ (**1**) and $[\text{Cu}(\text{bpba})_2(\text{H}_2\text{O})(\text{NO}_3)](\text{NO}_3) \cdot 2\text{H}_2\text{O} \cdot \text{MeOH}$ (**2**), are synthesized using bpba and their corresponding acetate and nitrate anions and characterized by elemental analyses, infrared (IR) spectroscopy, UV/vis spectroscopy, and single-crystal X-ray diffraction. Unexpectedly, the geometry adopted by the Cu(II) ion in **1** is a paddle-wheel dimeric unit, wherein the local geometry induces the formation of a zigzag 1D-chain structure. The photoluminescence properties of **1** and **2** are investigated, demonstrating their dependence on the counter-anions and bridging ligands. The magnetic properties of **1** and **2** are investigated and are dependent on the geometric structures around the Cu(II) ions.

2. Materials and Methods

2.1. General Information

Reagent grade chemicals were used in the synthesis without further purification. bpba was prepared according to a previously reported procedure [23]. IR spectra were recorded on a Thermo Fisher scientific IR200 spectrophotometer ($\pm 1 \text{ cm}^{-1}$) using a KBr disk (Thermo Fisher Scientific, Seoul, Korea). UV/vis absorption spectra were recorded using a SCINCO S-2100 spectrophotometer (Scinco, Seoul, Korea). To measure solid state UV/Vis spectra, compounds **1** and **2** were grounded in a mortar with pestle. The powder samples were made as round-shaped disks. Then, they were measured using reflectance method. Elemental analyses were performed using a Fisons/Carlo Erba EA1108 instrument (Thermo Fisher Scientific, Seoul, Korea). Thermogravimetric analysis (TGA) was performed at a scan rate of $5 \text{ }^\circ\text{C}/\text{min}$ using a Seiko TG/DTA 320 & SSC 5200H disk station system. The luminescence spectra were obtained using a SINCO FS-2 fluorescence spectrometer (Scinco, Seoul, Korea). The magnetic susceptibilities were measured in an applied field of 5000 Oe in the range of 5–300 K using a Quantum Design MPMS superconducting quantum interference device (SQUID) magnetometer (Quantum Design, San Diego, CA, USA). Diamagnetic corrections were made $[314.98$ (**1**) and 440.01×10^{-6} (**2**) $\text{emu}/\text{mol}]$ using Pascal's constants.

2.2. Syntheses

Preparation of $[\text{Cu}_2(\text{bpba})(\text{CH}_3\text{COO})_4]$ (**1**): A CH_3OH solution (5 mL) of $\text{Cu}(\text{CH}_3\text{COO})_2 \cdot \text{H}_2\text{O}$ (19 mg, 0.095 mmol) was added dropwise to a CH_3OH solution (5 mL) of bpba (25 mg, 0.095 mmol) [23]. The resulting green solution was stirred at room temperature for 30 min. After filtering, green crystals were obtained by the slow diffusion of diethyl ether into the solution, collected by filtration, washed with CH_3OH , and dried in air. Yield: 19 mg (63%). Anal. Calcd. for $\text{C}_{25}\text{H}_{27}\text{Cu}_2\text{N}_3\text{O}_8$: C, 48.07; H, 4.36; N, 6.73. Found: C, 47.68; H, 4.72; N, 6.42. IR (KBr): 3111, 3068, 3009, 2975, 2938, 2818, 1622, 1590, 1432, 1218, 1018 cm^{-1} .

Preparation of $[\text{Cu}(\text{bpba})_2(\text{H}_2\text{O})(\text{NO}_3)](\text{NO}_3) \cdot 2\text{H}_2\text{O} \cdot \text{MeOH}$ (**2**): A solution of $\text{Cu}(\text{NO}_3)_2 \cdot 3\text{H}_2\text{O}$ (17 mg, 0.061 mmol) in $\text{CH}_3\text{OH}/\text{H}_2\text{O}$ (4:1 v/v, 5 mL) was added dropwise to a solution of bis(4-pyridyl)benzylamine (32 mg, 0.122 mmol) in CH_3OH (5 mL) [23]. The resulting solution was allowed to stand at room temperature until blue crystals formed, which were then filtered off, washed with CH_3OH , and dried in air. Yield: 30 mg (55%). Anal. Calcd. for $\text{C}_{35}\text{H}_{38}\text{CuN}_8\text{O}_9$: C, 54.01; H, 4.92; N, 14.40. Found: C, 54.18; H, 4.68; N, 14.16. IR (KBr): 3439, 3094, 3074, 3045, 3015, 2926, 1624, 1601, 1508, 1384, 1215, 816 cm^{-1} .

2.3. X-ray Crystallography

Crystals of **1** and **2** were mounted on a CryoLoop[®] with Paratone[®] oil. The intensity data for the structures were collected using a Bruker APEX CCD-based diffractometer (Korea Basic Science Institute, Chonju Branch) and Mo-K α radiation ($\lambda = 0.71073 \text{ \AA}$, graphite

monochromator) (Bruker Korea, Seoul, Korea) at 200(2) K. The raw data were processed to obtain structure factors using the Bruker SAINT program and corrected for Lorentz and polarization effects [24]. The intensity data for **1** and **2** were corrected for absorption using the SADABS program with multi-scan data ($T_{\min}/T_{\max} = 0.837$ for **1** and 0.835 for **2**) [25]. The crystal structures were solved using direct methods [26] and refined by full-matrix least-squares refinement using the SHELXL-2018 computer program (Bruker Korea, Seoul, Korea) [27]. The positions of all non-hydrogen atoms were refined using anisotropic displacement factors. The benzyl group of **1** was symmetrically disordered; the occupancy of the benzyl groups was 0.5, which was refined. All hydrogen atoms were placed using a riding model and their positions were constrained relative to their parent atoms using the appropriate HFIX command in SHELXL-2018. The crystallographic data and results of the refinements for **1** and **2** are summarized in Table 1.

Table 1. Summary of the crystallographic data for polymers **1** and **2**.

Compound	1	2
Empirical formula	C ₂₅ H ₂₇ Cu ₂ N ₃ O ₈	C ₃₅ H ₄₀ CuN ₈ O ₁₀
Formula weight	624.58	796.29
Crystal system	Monoclinic	Monoclinic
Space group	C2/c	P2 ₁ /c
<i>a</i> , Å	14.737(1)	17.917(1)
<i>b</i> , Å	7.569(1)	12.966(1)
<i>c</i> , Å	25.6870(14)	17.518(1)
α , deg	90	90
β , deg	97.3060(10)	113.399(2)
γ , deg	90	90
<i>V</i> , Å ³	2842.0(3)	3735.0(6)
<i>Z</i>	4	4
<i>d</i> _{calc} , g cm ^{−3}	1.460	1.416
λ , Å	0.71073	0.71073
<i>T</i> , K	200(2)	200(2)
μ , mm ^{−1}	1.546	0.652
<i>F</i> (000)	1280	1660
Reflections collected/ $2\theta_{\max}$	9465/56.55	22,765/52.02
Independent reflections	3294	7321
Reflections with $I > 2\sigma(I)$	2048	4064
Goodness-of-fit on F^2	1.073	0.958
Final R indices [$I > 2\sigma(I)$] ^a	$R_1 = 0.0767$ $wR_2 = 0.1660$	$R_1 = 0.0628$ $wR_2 = 0.1621$
CCDC	2,183,299	2,183,300

$$^a R_1 = \sum ||F_o| - |F_c|| / \sum |F_o|, wR_2 = [\sum w(F_o^2 - F_c^2)^2 / \sum w(F_o^2)]^{1/2}.$$

3. Results and Discussion

3.1. Synthesis and Characterization

1 was prepared by way of the reaction of Cu(CH₃COO)₂·H₂O and the bpba ligand in a methanol solution under aerobic conditions at room temperature and a 63% yield was observed. Strong absorptions at 1590 (asymmetric stretching mode) and 1432 (symmetric stretching mode) cm^{−1}, owing to the acetate anions coordinated to the Cu(II) ion, were observed in the IR spectrum of **1** in KBr [28,29]. The signals for the C–H bonds of the bpba ligand were detected at 3111–2818 cm^{−1}. Furthermore, the pyridine peak ($\nu_{C=N}$) of the bpba ligand was observed at 1622 cm^{−1}. This is blue-shifted due to the coordination to Cu(II) ion, compared to that of bpba ligand (1604 cm^{−1}). A distinct absorption band in the range of 230–440 nm, with maxima at 262, 302 (sh), and 380 (sh) nm was observed in the UV/vis spectrum of **1** in the solid state, at room temperature. This UV/vis spectrum was similar to that of the free bpba ligand, where the peaks were attributed to the n– π^* and π – π^* transitions of the pyridine and benzene moieties [30]. That is, the peaks can be assigned as n– π^* (262 nm, benzyl), π – π^* (302 nm, 4,4'-bipyridylamine), and n– π^* transitions (380 nm,

4,4'-bipyridylamine), respectively. The d–d transition band of the Cu(II) ion was observed in the range of 550–970 nm, with a maximum at 752 nm (Figure 1) [31]. In **1**, the copper(II) ion is coordinated with four oxygen atoms from acetate ions in a square planar and one pyridine nitrogen atom in an axial position and has a coordination environment of CuO₄N.

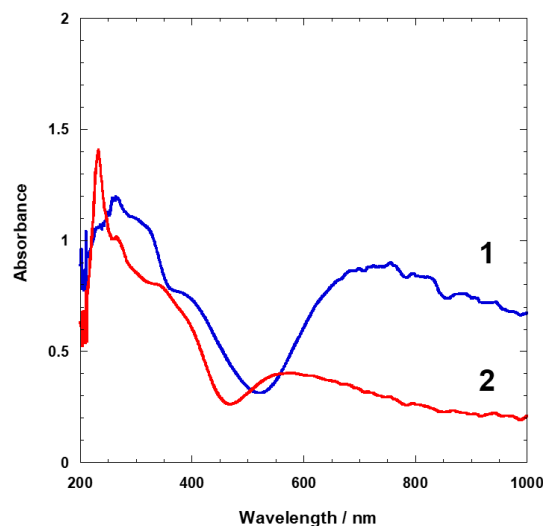


Figure 1. UV-Vis spectra of **1** (blue line) and **2** (red line) in the solid state.

2 was obtained by the reaction of Cu(NO₃)₂·3H₂O and the bpba ligand in a methanol/water solution under aerobic conditions at room temperature, and a 55% yield was observed. Strong absorption of the coordinated nitrate anions at 1384 cm⁻¹ (antisymmetric stretching mode) was observed in the IR spectrum of **2** in KBr [32]. The signals for the C–H bonds of the bpba ligand were detected at 3094–2926 cm⁻¹. Likewise, the ν_{C=N} peak was displayed at 1624 cm⁻¹, which is also blue-shifted to that of the bpba ligand by the coordination of Cu(II) ion. A distinct absorption band in the range of 215–430 nm, with maxima at 233, 265 (sh), and 338 (sh) was observed in the UV/vis spectrum of **2** in the solid state, at room temperature. This UV/vis spectrum was similar to that of the free bpba ligand, where the peaks were attributed to the n–π* and π–π* transitions of the pyridine and benzene moieties [30]. That is, the peaks can be assigned as π–π* (233 nm, benzyl), n–π* (265 nm, benzyl), and n–π*/π–π* transitions (338 nm, 4,4' bipyridylamine), respectively. The d–d transition band of the Cu(II) ion was observed in the range of 490–965 nm, with a maximum at 575 nm (Figure 1) [31]. In **2**, the Cu(II) ion is bonded with four nitrogen atoms from pyridine moieties in a square planar and two oxygen atoms from water molecule and nitrate ion in axial positions, which forms a CuN₄O₂ coordination environment. Thus, the coordination environments can be attributed to the difference of d–d transition band.

The TGA trace of **1** showed no decomposition up to 162 °C. The 5.45% weight loss in the range of 162–177 °C was attributed to the partial decomposition of the acetate group (Figure 2). Starting at 194 °C and continuing to 291 °C, **1** rapidly decomposed. From 291 to 500 °C, no weight loss was observed in the polymer, and the weight of the residue corresponded to that of Cu(II) oxide without any organic components [33,34]. The TGA trace of **2** showed 7.7% weight loss at 85 °C, corresponding to the loss of all solvents (i.e., H₂O and CH₃OH) per unit formula (Figure 2). No chemical decomposition was observed in **2** up to 228 °C; it rapidly decomposed above 228 °C. At approximately 400 °C, most of the organic components disappeared, and only Cu(II) oxide remained. **1** decomposed faster than **2**, indicating that **2** was more thermally stable than **1**.

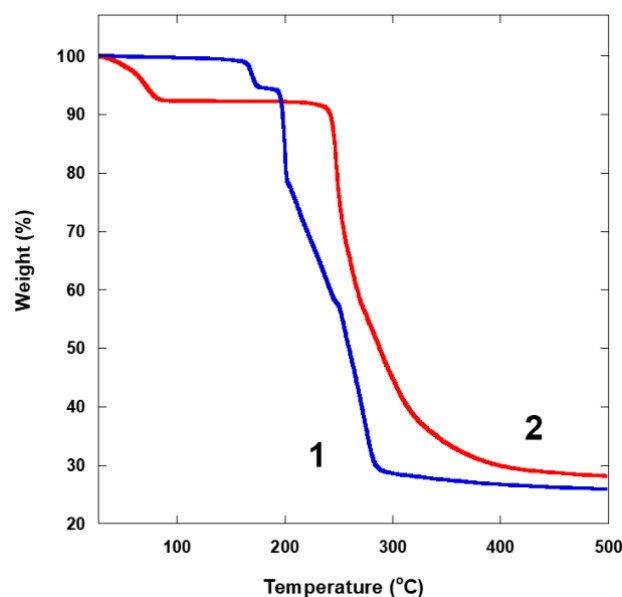


Figure 2. Thermogravimetric analysis (TGA) traces for **1** (blue line) and **2** (red line).

3.2. Description of the Crystal Structures

X-ray crystal structure of **1**: **1** crystallizes in the monoclinic $C2/c$ -space group; the crystallographic data and results of the refinements are summarized in Table 1. An ORTEP diagram of **1** is shown in Figure 3, and Table 2 lists the selected bond lengths and angles. The asymmetric unit of **1** is composed of one Cu(II) ion, a half-bpba ligand, and two acetate ions. The Cu(II) center is pentacoordinated as CuNO_4 in a distorted square pyramidal coordination sphere and is bonded to the four oxygen atoms of the four acetate ligands and one nitrogen donor atom of one bpba ligand. The Cu1 ion is displaced from the equatorial plane toward the nitrogen atom of bpba by 0.197(2) Å. The Cu1...Cu1' distance in the paddle-wheel geometry is 2.621(1) Å, corresponding to a weak cuprophilic interaction. This distance falls within the range observed for other similar species [35]. Consequently, the geometry of the paddle-wheel Cu_2 unit can be described as a pseudo-octahedral species. The average Cu–N and Cu–O bond distances are 2.175(5) and 1.980(2) Å, respectively. These values lie within the range for Cu–N or Cu–O single bonds calculated from the crystallographic data [36,37]. Owing to the Jahn–Teller distortion, the axial bonds are somewhat longer than the equatorial bonds. The bond angle around Cu(II) is 88.2(2)–168.7(2). These values fall within the range for normal square pyramidal Cu(II) compounds [38,39].

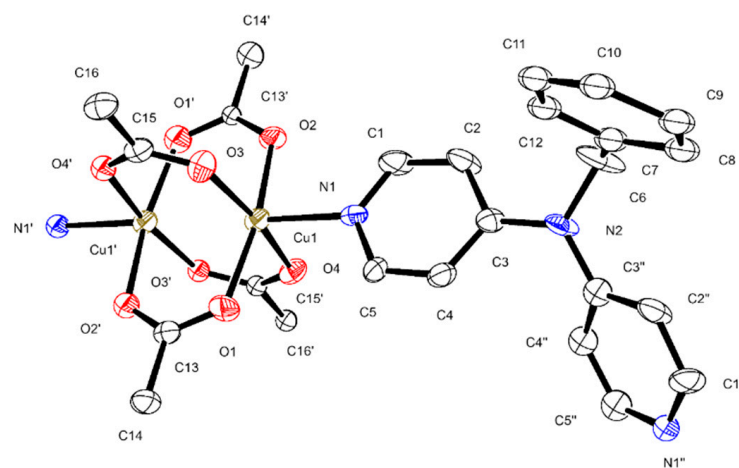


Figure 3. ORTEP drawing of polymer **1**. The thermal ellipsoids are shown at 30% level. The hydrogen atoms and disordered benzyl group are omitted for clarity ($' = -x, -y, -x + 1$; $'' = -x, y, -z + 3/2$).

Table 2. Selected bond distances (Å) and angles (°) for polymers 1 and 2.

1		2	
Cu1–N1	2.175(5)	Cu1–N1	2.045(4)
Cu1–O1	1.990(4)	Cu1–N4	2.009(4)
Cu1–O2	1.963(4)	Cu1–N3'	2.023(4)
Cu1–O3	1.975(4)	Cu1–N6''	2.045(4)
Cu1–O4	1.993(4)	Cu1–O1	2.367(3)
Cu1–Cu1'	2.621(2)	Cu1–O2	2.644(4)
N1–Cu1–O1	95.83(19)	N1–Cu1–O1	89.00(13)
N1–Cu1–O2	95.68(19)	N4–Cu1–O1	94.67(13)
N1–Cu1–O3	94.92(18)	N3'–Cu1–O1	92.21(13)
N1–Cu1–O4	96.39(18)	N6''–Cu1–O1	91.29(13)
O1–Cu1–O2	168.4(2)	N1–Cu1–N4	176.27(15)
O1–Cu1–O3	90.4(2)	N1–Cu1–N3'	90.22(15)
O1–Cu1–O4	88.2(2)	N1–Cu1–N6''	89.81(15)
O2–Cu1–O3	89.69(18)	N4–Cu1–N3'	90.33(15)
O2–Cu1–O4	89.50(18)	N4–Cu1–N	89.42(15)
O3–Cu1–O4	168.68(19)	N3'–Cu1–N6''	176.50(15)

Symmetric transformations used to generate equivalent atoms: (') $-x, -y, -z + 1$ for polymer 1 and (') $x, -y - 1/2, z - 1/2$; (') $x, -y + 1/2, z + 1/2$ for polymer 2.

In **1**, the two pyridine groups of the bpba ligand are twisted at an angle of $54.4(2)^\circ$, which is related to N2. The two pyridyl nitrogen atoms of the bpba ligand are coordinated to two different Cu(II) ions. Therefore, the Cu(II) atoms and bpba ligands are linked alternatively to afford a 1D zigzag structure along the *c*-axis (Figure 4) [40]. That is, the 1D chain exhibits a linear structure with a zigzag pitch of 25.860 \AA along the axis. The nearest Cu...Cu separation between the 1D chains is $6.446(2) \text{ \AA}$, and the nearest Cu...Cu separation within the 1D chain is $10.691(2) \text{ \AA}$. Between the 1D chains, herringbone-stacking interactions are formed between the benzyl group of bpba and the pyridine group of bpba belonging to adjacent 1D chains, giving rise to a 2D network (Figure 4). The distance between the centroids is 4.820 \AA , and the dihedral angle between the benzyl and pyridine groups of bpba is $86.2(3)$.

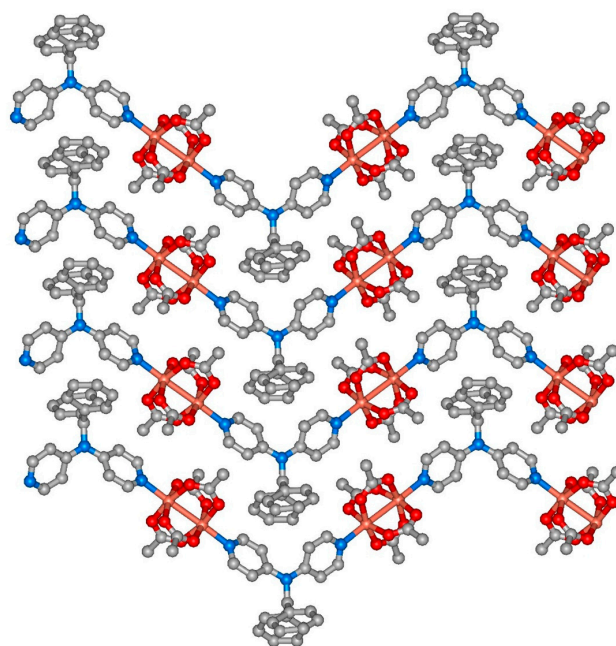


Figure 4. Extended 2D structure of polymer 1 displaying the π - π interactions through the benzyl and pyridine groups between the 1D chains. Both positions of the disordered benzyl group are shown, each in a 50% proportion.

X-ray crystal structure of **2**: Compound **2** crystallizes in the monoclinic $P2_1/c$ space group; the crystallographic data and the results of the refinements are summarized in Table 1. An ORTEP diagram of **2** is shown in Figure 5, and Table 2 lists the selected bond lengths and angles. The asymmetric unit of **2** is composed of one Cu(II) ion, two bpba ligands, two nitrate ions, three water molecules, and one methanol molecule. The Cu(II) cation is hexacoordinated as CuN_4O_2 in a distorted octahedral structure and is bonded to the four pyridyl nitrogen atoms of the four bpba ligands, one water oxygen atom, and one oxygen atom of one nitrate anion. The average Cu–N and Cu–O bond distances are 2.031(2) and 2.467(2) Å, respectively. The bond angles around Cu(II) are 89.0(1)–176.5(1). These values are within the range for normal octahedral Cu(II) compounds [37,40]. In **2**, each pyridine group in the two bpba ligands in the structure is twisted, with angles of 58.0(2) and 72.8(2)°, related to N2 and N5, respectively. The two pyridyl nitrogen atoms of the bpba ligand are coordinated to two different Cu(II) ions. Each Cu(II) ion is coordinated to four different bpba ligands. Therefore, the Cu(II) atoms and bpba ligands are linked alternatively to afford a 2D grid structure. This 2D layer is packed along the *a* axis, with an interlayer distance of 8.22 Å. Because each Cu(II) ion is bonded to four bpba ligands, and each bpba binds to two Cu(II) ions, the stoichiometry of the polymer complex corresponds to $\text{Cu}^{2+}/\text{bpba} = 1:2$, which generates 2D layers extending along the *b* + *c* plane (Figure 6). The 2D layer is composed of rings that include 40 atoms from four Cu(II) ions and four bpba ligands. The nearest Cu···Cu separation between the 2D layers is 10.961(2) Å, and the nearest Cu···Cu separation within the 2D layer is 10.755(2) Å.

Two benzyl groups of two bpba ligands in the asymmetric unit of **2** (Figure 6) are involved in offset-stacking and herringbone $\pi\pi-\pi$ interactions with benzyl and pyridine groups belonging to other Cu(II) ions [41]. For example, one benzyl group with C15 shows offset-stacking interactions with different benzyl groups with C15 ($-x, -y - 1, -z + 1$) (interplanar separation: 3.473(9)–3.489(9) Å, centroid···centroid 4.621 Å) and herringbone $\pi-\pi$ interaction with different pyridine groups with N3 ($-x, -y - 1, -z + 1$) (dihedral angle 88.4(2)°; centroid···centroid 5.017 Å). The other benzyl group with C32 displays a herringbone interaction with different pyridine groups with N4 ($-x + 1, y - 1/2, -z + 1/2$) (dihedral angle 43.4(2)°; centroid···centroid 4.922 Å). Furthermore, two strong hydrogen bonding interactions are observed between the oxygen of the coordinated water molecule, the oxygen atom of the free nitrate ion, and the oxygen atom of the methanol molecule (O1···O6(NO_3^-): 2.830 Å, O1···O8(MeOH): 2.736 Å).

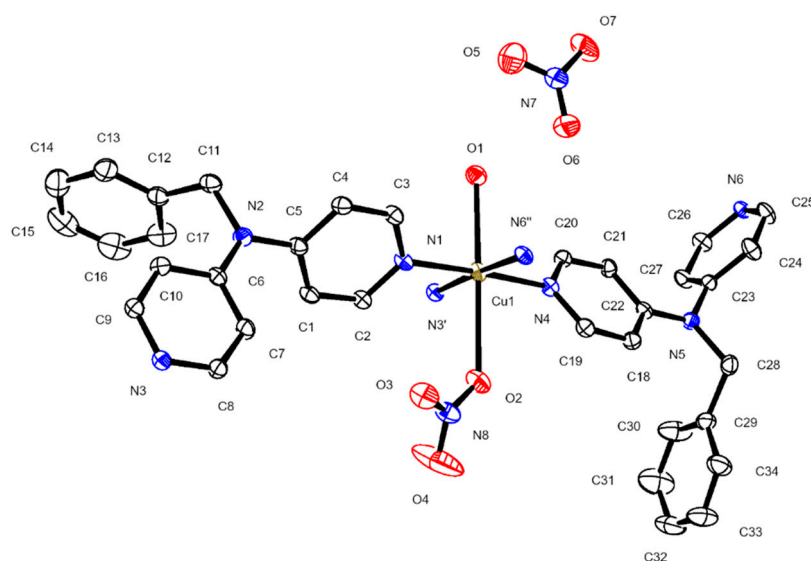


Figure 5. ORTEP drawing of polymer **2**. The thermal ellipsoids are shown at 30% level. The solvent molecules and hydrogen atoms are omitted for clarity.

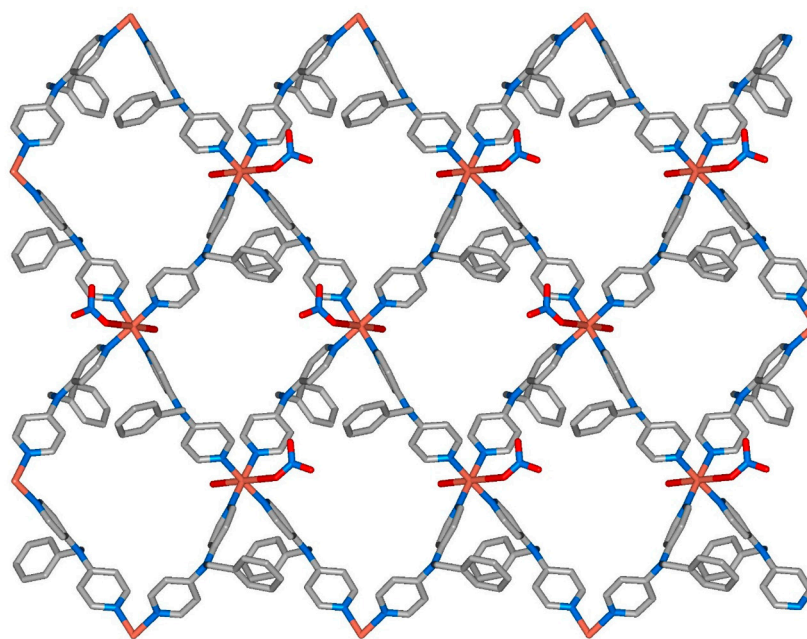


Figure 6. Extended 2D structure of polymer **2** formed by the coordination of the Cu(II) ions and bpba ligands.

3.3. Photoluminescence Properties of **1** and **2**

Photoluminescence spectra of **1** and **2** in the solid state were obtained under aerobic conditions at room temperature. Upon excitation at 300 nm, strong emission bands with maxima at 355 and 466 nm were observed for **1** and one band was observed at 464 nm for **2** (Figure 7). Unexpectedly, we could observe strong photoluminescence emissions in **1** and **2**, even though the polymers have a strong quencher of Cu(II) ion [42,43]. The bpba ligand exhibited emission bands at 346 and 448 nm upon excitation at 300 nm, which were attributed to the $\pi \rightarrow \pi^*$ or $\pi \rightarrow n$ transitions of the benzene and pyridine groups [44,45]. For the bpba ligand, the intensity of the benzene group was higher than that of the pyridine group in the solid state. Compared to the emission peaks of bpba, those of **1** were red-shifted by approximately 9 and 18 nm, respectively. In this case, the longer-wavelength emission was more significant than the shorter-wavelength emission. This behavior was opposite to that of the bpba ligand. Remarkably, **2** exhibited only one emission band at 464 nm. The shorter-wavelength emission at approximately 350 nm disappeared owing to the geometry and anion. The emission of **2** at approximately 464 nm was red-shifted by approximately 16 nm for the bpba ligand. The long-wavelength emission at approximately 464 nm in **2** became significantly more intense, accompanied by band broadening compared to that of **1**, because of the vibration of the methanol and water molecules. Generally, the photoluminescence of the coordination polymers depends on the type of metal ion [46–50]. Interestingly, different behaviors related to quenching of the emissions in **1** and **2** were observed in the solid state. In contrast to **2**, the coordination polymer [(bpba)Zn(CH₃COO)₂]_n showed a strong emission band at 361 nm without any emission at approximately 460 nm [44]. Therefore, this difference could potentially be utilized to control and select the emission wavelengths for optical materials. In the case of **1** and **2** as well as silver(I) coordination polymers [Ag(bpba)(CF₃SO₃)]·CH₃CN and [Ag₂(bpba)₂(NO₃)₂]·CH₃CN·H₂O [23], the emission shifts to bpba ligand were relatively small in **1** and **2**, indicating that the Cu(II) ion was comparatively a weak interaction (i.e., π back donation) with bpba compared to the silver(I) ion.

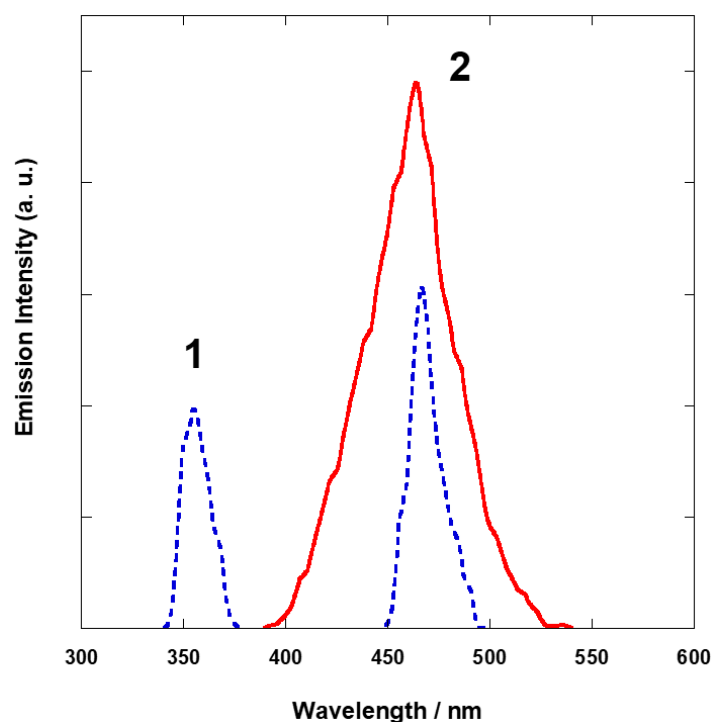


Figure 7. Photoluminescence spectra ($\lambda_{ex} = 300$ nm) of polymers **1** (dotted line, blue) and **2** (solid line, red).

3.4. Magnetic Properties of **1** and **2**

The magnetic susceptibilities of **1** and **2** were measured on solid samples in an applied field of 5000 Oe between 5 and 300 K and plotted as $\chi_M T$ vs. T (Figure 8). For **1**, the effective magnetic moment at 300 K was $2.06 \mu_B/\text{Cu}_2$, which was significantly lower than the value ($2.83 \mu_B/\text{Cu}_2$) expected for two independent $S = 1/2$ Cu(II) spins ($g = 2.0$). The value of $\mu_{\text{eff}}(T)$ decreased gradually to $0.277 \mu_B/\text{Cu}_2$ with a decrease in the temperature to 5 K, indicating a strong antiferromagnetic interaction within the $\text{Cu}^{\text{II}}-(\eta^2\text{-OAc})_4\text{-Cu}^{\text{II}}$ unit. Interestingly, the effective moment decreased gradually when the temperature was raised to 80 K, and then decreased linearly when it was decreased to 5 K. Considering the structure of **1**, the magnetic data were fitted to the analytical expression (the Bleaney–Bowers equation) for a coupled $S = 1/2$ ($S_1 = S_2 = 1/2$) dinuclear spin model ($H = -2J(\hat{S}_1 \cdot \hat{S}_2) + g\beta\hat{S} \cdot B$) [51,52]. The best fit gave values of $J = -172 \text{ cm}^{-1}$, $g = 2.27$, $\theta = -6.5 \text{ K}$, $p = 0.027$, and $\text{tip} = 240 \times 10^{-6} \text{ emu/mol}$ (where p is the molar fraction of non-coupled species; θ is the interdimer interaction; tip is the temperature-independent paramagnetism). As expected, **1** exhibited strong antiferromagnetic coupling within the dimeric unit and very weak antiferromagnetic interaction between the dimeric units within the 1D chain and/or between the 1D chains. The J value (-172 cm^{-1}) was smaller than that of $\text{Cu}_2(\text{CH}_3\text{COO})_4 \cdot 2\text{H}_2\text{O}$ ($J = -290 \text{ cm}^{-1}$) [53], attributed to the coordination of the bpba ligand between the dimeric Cu units. Due to the coordination, the Cu–Cu bond distance was altered ($\sim 0.02 \text{ \AA}$), which might be influenced by the order of orbital overlap. Furthermore, the coupling constant of **1** was comparable to -166 and -175 cm^{-1} for $[\text{Cu}_2(\text{histamine})_2(\text{C}_2\text{O}_4)(\text{ClO}_4)_2]$ and $[\text{Cu}_2(\text{mepirizole})_2(\text{C}_2\text{O}_4)(\text{ClO}_4)_2]$, respectively, although the bridging ligands were very different [54,55].

The effective magnetic moment of **2** at 300 K was $1.96 \mu_B/\text{Cu}$ and remained almost constant with a decrease in the temperature to 15 K ($1.96 \mu_B/\text{Cu}$). This value of $\mu_{\text{eff}}(T)$ at 300 K was slightly higher than the expected spin-only value of $1.73 \mu_B/\text{Cu}$ and was attributed to a small effective g value, i.e., $g_{\text{eff}} = 2.26$ ($\mu_{\text{eff}} = g_{\text{eff}}[S(S+1)]^{1/2}$, S = total-spin angular momentum quantum number). Below 15 K, $\mu_{\text{eff}}(T)$ decreased, reaching $1.91 \mu_B/\text{Cu}$ at 5 K, which could be attributed to the intermolecular interactions between the Cu(II) ions [56,57]. In the 2D framework of **2**, the inter Cu distances through the 4, 4'-bipyridylamine unit

of the bpba ligand were very long. Thus, the magnetic interactions between the Cu(II) ions within the 2D framework were not efficient. From this perspective, the Cu(II)–Cu(II) interactions in **2** were favorable through space rather than bonding. Additionally, above 5 K, $\chi_M^{-1}(T)$ can be fit to the Curie–Weiss expression $\chi_M = C/(T-\theta)$ with $\theta = -0.40$ K ($C = 0.469$ emu K/mol) for **2** [51]. The Weiss constant indicates weak antiferromagnetic interactions within and/or between the 2D coordination polymer networks of **2**.

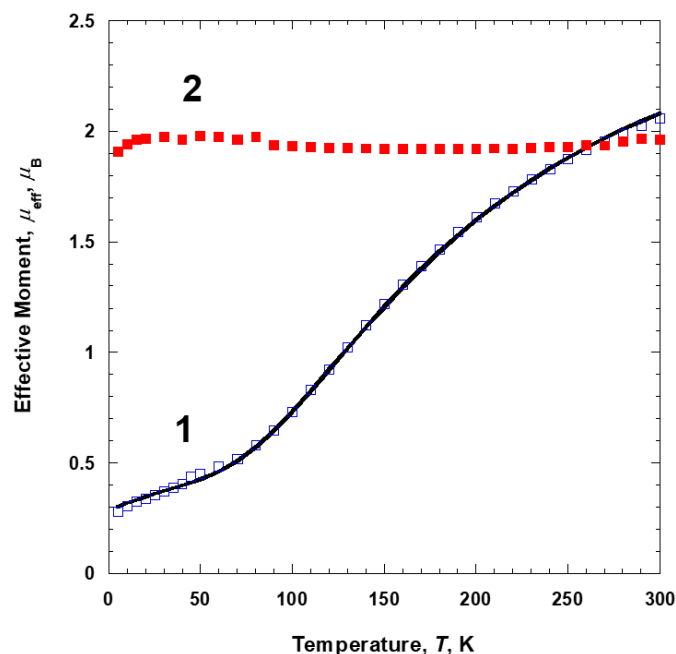


Figure 8. Temperature-dependence of the magnetic moments of polymers **1** (□, blue) and **2** (■, red). The solid line represents a best fit of the data as described in the text.

4. Conclusions

Two novel bpba-based Cu(II) coordination polymers with unusual emission behaviors and unique magnetic properties, depending on the geometric structure, were presented. The Cu(II) ions of **1** and **2** formed a paddle-wheel structure with bridging acetates and adopted octahedral geometry with four pyridine groups, one water molecule, and one methanol molecule, respectively. By connecting Cu(II) ions and bpba ligands, **1** and **2** exhibited a zigzag 1D chain structure with paddle-wheel moieties and a puckered 2D network structure with a distorted square shape, respectively. **1** and **2** displayed slightly red-shifted emissions compared to those of the bpba ligand because of the presence of Cu(II) and counter ions. Interestingly, **2** showed strong emission at 464 nm only, with no emission at approximately 350 nm. **1** showed a strong antiferromagnetic interaction within the paddle-wheel unit, whereas **2** displayed very weak antiferromagnetic coupling through the bipyridine unit and/or space.

Author Contributions: I.U., J.W.S., R.T., S.H. and H.J.S. did the experiments and analyzed the data. K.S.M. charged the project. All authors have read and agreed to the published version of the manuscript.

Funding: This research was funded by the National Research Foundation of Korea (Nos. 2018R1D1A1B07043305 and 2021R1F1A1062108).

Institutional Review Board Statement: Not applicable.

Informed Consent Statement: Not applicable.

Data Availability Statement: Supplementary crystallographic data can be obtained free of charge online at <http://www.ccdc.cam.ac.uk/conts/retrieving.html> (accessed on 1 July 2022).

Acknowledgments: This research was supported by the Basic Science Research Program (Nos. 2018R1D1A1B07043305 and 2021R1F1A1062108) through the National Research Foundation of Korea (NRF).

Conflicts of Interest: The authors declare no conflict of interest.

References

1. Li, G.; Han, Y. Two-in-One MOF Structure with Tunable Porosity for Enhanced Separation. *ACS Cent. Sci.* **2022**, *8*, 150–152. [[CrossRef](#)]
2. Du, R.; Wu, Y.; Yang, Y.; Zhai, T.; Zhou, T.; Shang, Q.; Zhu, L.; Shang, C.; Guo, Z. Porosity Engineering of MOF-Based Materials for Electrochemical Energy Storage. *Adv. Energy Mater.* **2021**, *11*, 2100154. [[CrossRef](#)]
3. Jeong, A.R.; Shin, J.W.; Jeong, J.H.; Jeoung, S.; Moon, H.R.; Kang, S.; Min, K.S. Porous and nonporous coordination polymers induced by pseudohalide ions for luminescence and gas sorption. *Inorg. Chem.* **2020**, *59*, 15987–15999. [[CrossRef](#)] [[PubMed](#)]
4. Samanta, P.; Let, S.; Mandal, W.; Dutta, S.; Ghosh, S.K. Luminescent metal–organic frameworks (LMOFs) as potential probes for the recognition of cationic water pollutants. *Inorg. Chem. Front.* **2020**, *7*, 1801–1821. [[CrossRef](#)]
5. Lee, K.; Park, J.; Song, I.; Yoon, S.M. The Magnetism of Metal–Organic Frameworks for Spintronics. *Bull. Korean Chem. Soc.* **2021**, *42*, 1170–1183. [[CrossRef](#)]
6. Thorarinsdottir, A.E.; Harris, T.D. Metal–Organic Framework Magnets. *Chem. Rev.* **2020**, *120*, 8716–8789. [[CrossRef](#)]
7. Shao, L.; Hu, X.; Sikligar, K.; Baker, G.A.; Atwood, J.L. Coordination Polymers Constructed from Pyrogallol[4]arene-Assembled Metal–Organic Nanocapsules. *Acc. Chem. Res.* **2021**, *54*, 3191–3203. [[CrossRef](#)]
8. Persson, I.; Persson, P.; Sandström, M.; Ullström, A.-S. Structure of Jahn–Teller distorted solvated copper(II) ions in solution, and in solids with apparently regular octahedral coordination geometry. *J. Chem. Soc. Dalton Trans.* **2002**, 1256–1265. [[CrossRef](#)]
9. Trivedi, M.; Yadav, A.K.; Singh, G.; Kumar, A.; Kumar, G.; Husain, A.; Rath, N.P. Synthetic, spectral, structural and catalytic activity of infinite 3-D and 2-D copper(II) coordination polymers for substrate size-dependent catalysis for CO₂ conversion. *Dalton Trans.* **2019**, *48*, 10078–10088.
10. Hussain, N.; Bhardwaj, V.K. The influence of different coordination environments on one-dimensional Cu(II) coordination polymers for the photo-degradation of organic dyes. *Dalton Trans.* **2016**, *45*, 7697–7707. [[CrossRef](#)]
11. Wang, X.-P.; Zhao, Y.-Q.; Jagličić, Z.; Wang, S.-N.; Lin, S.-J.; Li, X.-Y.; Sun, D. Controlled *in situ* reaction for the assembly of Cu(II) mixed-ligand coordination polymers: Synthesis, structure, mechanistic insights, magnetism and catalysis. *Dalton Trans.* **2015**, *44*, 11013–11020. [[CrossRef](#)] [[PubMed](#)]
12. Köberl, M.; Cokoja, M.; Herrmann, W.A.; Kühn, F.E. From molecules to materials: Molecular paddle-wheel synthons of macromolecules, cage compounds and metal–organic frameworks. *Dalton Trans.* **2011**, *40*, 6834–6859. [[CrossRef](#)] [[PubMed](#)]
13. Muhammad, N.; Ikram, M.; Rehman, S.; Ali, S.; Akhtar, M.N.; AlDamen, M.A.; Schulzke, C. A paddle wheel dinuclear copper(II) carboxylate: Crystal structure, thermokinetic and magnetic properties. *J. Mol. Struct.* **2019**, *1196*, 754–759.
14. Nesterova, O.V.; Kirillova, M.V.; Guedes da Silva, M.F.C.; Boča, R.; Pombeiro, A.J.L. How to force a classical chelating ligand to a metal non-chelating bridge: The observation of a rare coordination mode of diethanolamine in the 1D complex {[Cu₂(Piv)₄(H₃tBuDea)](Piv)}_n. *CrystEngComm* **2014**, *16*, 775–783. [[CrossRef](#)]
15. Soldevila-Sanmartín, J.; Ayllón, J.A.; Calvet, T.; Font-Bardia, M.; Domingo, C.; Pons, J. Synthesis, crystal structure and magnetic properties of a Cu(II) paddle-wheel complex with mixed bridges. *Inorg. Chem. Commun.* **2016**, *71*, 90–93. [[CrossRef](#)]
16. Mahmoudi, G.; Masoudiasl, A.; Afkhami, F.A.; White, J.M.; Zangrando, E.; Gurbanov, A.V.; Frontera, A.; Safin, D.A. A new coordination polymer constructed from Pb(NO₃)₂ and a benzylideneisonicotinohydrazide derivative: Coordination-induced generation of a π -hole towards a tetrel-bonding stabilized structure. *J. Mol. Struct.* **2021**, *1234*, 130139. [[CrossRef](#)]
17. Jeong, A.R.; Shin, H.J.; Jang, Y.J.; Min, K.S. Two-dimensional zinc(II) and copper(I) coordination polymers for photoluminescence. *J. Mol. Struct.* **2022**, *1251*, 132031. [[CrossRef](#)]
18. Shin, J.W.; Bae, J.M.; Kim, C.; Min, K.S. Three-Dimensional Zinc(II) and Cadmium(II) Coordination Frameworks with *N,N,N',N'*-Tetrakis(pyridin-4-yl)methanediamine: Structure, Photoluminescence, and Catalysis. *Inorg. Chem.* **2013**, *52*, 2265–2267. [[CrossRef](#)]
19. Yang, W.; Yi, F.-Y.; Li, X.-D.; Wang, L.; Dang, S.; Sun, Z.-M. Construction of Cu(II) coordination polymers based on semi-rigid tetrahedral pyridine ligands. *RSC Adv.* **2013**, *3*, 25065–25070. [[CrossRef](#)]
20. Winter, S.; Weber, E.; Eriksson, L.; Csöreg, I. New coordination polymer networks based on copper(II) hexafluoroacetylacetonate and pyridine containing building blocks: Synthesis and structural study. *New J. Chem.* **2006**, *30*, 1808–1819. [[CrossRef](#)]
21. Fan, Y.-H.; Wang, J.-L.; Bai, Y.; Dang, D.B.; Zhao, Y.-Q. Two copper coordination polymers with pyridine imine-based ligand: Synthesis, crystal structure and luminescent properties. *Synth. Met.* **2012**, *162*, 1126–1132. [[CrossRef](#)]
22. Ding, B.; Wu, J.; Wu, X.X.; Huo, J.Z.; Zhu, Z.Z.; Liu, Y.Y.; Shi, F.X. Syntheses, structural diversities and characterization of a series of coordination polymers with two isomeric oxadiazol-pyridine ligands. *RSC Adv.* **2017**, *7*, 9704–9718. [[CrossRef](#)]
23. Shin, J.W.; Cho, H.J.; Min, K.S. Synthesis, structure and photoluminescence properties of silver(I) coordination polymers with bis(4-pyridyl)benzylamine. *Inorg. Chem. Commun.* **2012**, *16*, 12–16. [[CrossRef](#)]
24. *Saint Plus*, Version 6.02; Bruker Analytical X-ray: Madison, WI, USA, 1999.
25. *SADABS*, Version 2.03; Bruker AXS Inc.: Madison, WI, USA, 2000.
26. Sheldrick, G.M. Phase annealing in SHELX-90: Direct methods for larger structures. *Acta Cryst.* **1990**, *A46*, 467–473. [[CrossRef](#)]

27. Sheldrick, G.M. Crystal structure refinement with SHELXL. *Acta Cryst.* **2015**, *C71*, 3–8.
28. Nakamoto, K. 2. Application in Organometallic Chemistry. In *Infrared and Raman Spectra of Inorganic and Coordination Compounds*, 6th ed.; WILEY: Hoboken, NJ, USA, 2009; Volume 2, pp. 288–290.
29. Zeybel, L.; Köse, D.A. Acesulfame complex compounds of some lanthanide group metal cations. Synthesis and characterization. *J. Mol. Struct.* **2021**, *1226*, 129399. [[CrossRef](#)]
30. Pagliai, M.; Mancini, G.; Carnimeo, I.; De Mitri, N.; Barone, V. Electronic absorption spectra of pyridine and nicotine in aqueous solution with a combined molecular dynamics and polarizable QM/MM approach. *J. Comput. Chem.* **2017**, *38*, 319–335. [[CrossRef](#)]
31. Figgis, B.N.; Hitchman, M.A. *Ligand Field Theory and Its Applications*; Wiley-VCH: New York, NY, USA, 2000.
32. Nakamoto, K. 1. Applications in Coordination Chemistry. In *Infrared and Raman Spectra of Inorganic and Coordination Compounds*, 6th ed.; Wiley: Hoboken, NJ, USA, 2009; Volume 1, pp. 92–94.
33. Uysal, S.; Kurşunlu, A.N. The Synthesis and characterization of star shaped metal complexes of triazine cored schiff bases: Their thermal decompositions and magnetic moment values. *J. Inorg. Organomet. Polym.* **2011**, *21*, 291–296. [[CrossRef](#)]
34. Kocuyigit, O.; Kursunlu, A.N.; Guler, E. Complexation properties and synthesis of a novel Schiff base with triphenylene nucleus. *J. Hazard. Mater.* **2010**, *183*, 334–340. [[CrossRef](#)]
35. Appavoo, D.; Spencer, L.C.; Guzei, I.A.; Gomez-Garcia, C.J.; van Wyk, J.L.; Darkwa, J. Ring opening polymerization of D,L-lactide and ϵ -caprolactone catalysed by (pyrazol-1-yl)copper(II) carboxylate complexes. *RSC Adv.* **2021**, *11*, 13475–13485. [[CrossRef](#)]
36. Mastropietro, T.F.; Armentano, D.; Grisolia, E.; Zanchini, C.; Lloret, F.; Julve, M.; De Munno, G. Guanine-containing copper(II) complexes: Synthesis, X-ray structures and magnetic properties. *Dalton Trans.* **2008**, 514–520. [[CrossRef](#)] [[PubMed](#)]
37. Chun, M.K.; Jeong, A.R.; Min, K.S.; Jeong, J.H. Synthesis, crystal structure, and magnetic property of a stepped tetranuclear copper(II) complex of 3,5-diisopropylpyrazole-1-methoxide. *Inorg. Chem. Comm.* **2017**, *78*, 82–84. [[CrossRef](#)]
38. Shabana, S.Y.; Ramadan, A.M.; Ibrahim, M.M.; Elshami, F.I.; van Eldik, R. Square planar versus square pyramidal copper(II) complexes containing N3O moiety: Synthesis, structural characterization, kinetic and catalytic mimicking activity. *Inorg. Chim. Acta* **2019**, *486*, 608–616. [[CrossRef](#)]
39. Yu, F.; Ji, B.-Q.; Jagodič, M.; Su, Y.-M.; Zhang, S.S.; Feng, L.; Kurmoo, M.; Jagličić, Z.; Sun, D. Copper(II)-Assisted Ligand Fragmentation Leading to Three Families of Metallamacrocycle. *Inorg. Chem.* **2020**, *59*, 13524–13532. [[CrossRef](#)]
40. Park, H.W.; Sung, S.M.; Min, K.S.; Bang, H.; Suh, M.P. 1-D Zigzag Coordination Polymers of Copper(II) and Nickel(II) with Mixed Ligands: Syntheses and Structures. *Eur. J. Inorg. Chem.* **2001**, 2857–2863. [[CrossRef](#)]
41. Min, K.S.; Suh, M.P. Self-Assembly and Selective Guest Binding of Three-Dimensional Open-Framework Solids from Macrocyclic Complex as a Trifunctional Metal Building. *Chem. Eur. J.* **2001**, *7*, 303–313. [[CrossRef](#)]
42. Veselska, O.; Cai, L.; Podbevšek, D.; Ledoux, G.; Guillou, N.; Pilet, G.; Fateeva, A.; Demessence, A. Structural Diversity of Coordination Polymers Based on a Heterotopic Ligand: Cu(II)-Carboxylate vs Cu(I)-Thiolate. *Inorg. Chem.* **2018**, *57*, 2736–2743. [[CrossRef](#)]
43. Hazra, M.; Dolai, T.; Pandey, A.; Dey, S.K.; Patra, A. Fluorescent copper(II) complexes: The electron transfer mechanism, interaction with bovine serum albumin (BSA) and antibacterial activity. *J. Saudi Chem. Soc.* **2017**, *21*, S240–S247. [[CrossRef](#)]
44. Jeong, A.R.; Min, K.S. Zinc(II) and cadmium(II) coordination polymers with bis(4-pyridyl)benzylamine: Structure and photoluminescence. *J. Incl. Phenom. Macrocycl. Chem.* **2021**, *101*, 243–252. [[CrossRef](#)]
45. Lorenza, V.; Liebing, P.; Suta, M.; Engelhardt, F.; Hilfert, L.; Busse, S.; Wang, S.; Wickleder, C.; Edelmann, F.T. Synthesis, structure, complexation, and luminescence properties of the first metal-organic curcumin compound bis(4-triphenylsiloxy)curcumin. *J. Lumin.* **2019**, *211*, 243–250. [[CrossRef](#)]
46. Chumakov, Y.R.; Danilescu, O.; Kulikova, O.V.; Bourosh, P.; Bulhac, I.; Croitor, L. Metal ions impact on the isostructurality and properties of 2D coordination polymers. *CrystEngComm* **2022**, *24*, 4430–4439. [[CrossRef](#)]
47. Shi, X.; Qu, X.; Chai, J.; Tong, C.; Fan, Y.; Wang, L. Stable coordination polymers with linear dependence color tuning and luminescent properties for detection of metal ions and explosives. *Dye. Pigment.* **2019**, *170*, 107583. [[CrossRef](#)]
48. Nath, J.K.; Mondal, A.; Powell, A.K.; Baruah, J.B. Structures, Magnetic Properties, and Photoluminescence of Dicarboxylate Coordination Polymers of Mn, Co, Ni, Cu Having *N*-(4-Pyridylmethyl)-1,8-naphthalimide. *Cryst. Growth Des.* **2014**, *14*, 4735–4748. [[CrossRef](#)]
49. Kursunlu, A.N.; Baslak, C. A Bodipy-bearing pillar[5]arene for mimicking photosynthesis: Multi-fluorophoric light harvesting system. *Tetrahedron Lett.* **2018**, *59*, 1958–1962. [[CrossRef](#)]
50. Yoon, S.; Kim, H.-C.; Kim, Y.; Huh, S. Photophysical Properties and Electrochromism of Viologen Encapsulated Viologen@InBTB Metal–Organic Framework. *Bull. Korean Chem. Soc.* **2021**, *42*, 326–332. [[CrossRef](#)]
51. Kahn, O. *Molecular Magnetism*; VCH: New York, NY, USA, 1993.
52. Shin, J.W.; Jeong, A.R.; Hayami, S.; Moon, D.; Min, K.S. Synthesis, structure, and magnetic properties of dicopper and tricobalt complexes based on *N*-(2-pyridylmethyl)iminodiethanol. *Inorg. Chem. Front.* **2015**, *2*, 763–770. [[CrossRef](#)]
53. Güdel, H.U.; Stebler, A.; Furrer, A. Direct Observation of Singlet-Triplet Separation in Dimeric Copper(II) Acetate by Neutron Inelastic Scattering Spectroscopy. *Inorg. Chem.* **1979**, *18*, 1021–1023. [[CrossRef](#)]
54. Min, K.S.; Suh, M.P. Self-Assembly, Structures, and Magnetic Properties of Ladder-Like Copper(II) Coordination Polymers. *J. Solid State Chem.* **2000**, *152*, 183–190. [[CrossRef](#)]

55. Soto, L.; Garcia, J.; Escriva, E.; Legros, J.-P.; Tuchagues, J.-P.; Dahan, F.; Fuertes, A. Synthesis, Characterization, and Magnetic Properties of μ -Oxalato- and μ -Oxamido-Bridged Copper(II) Dimers. Crystal and Molecular Structures of $[\text{Cu}_2(\text{mepirizole})_2(\text{C}_2\text{O}_4)(\text{H}_2\text{O})_2](\text{PF}_6)_2 \cdot \text{mepirizole} \cdot 3\text{H}_2\text{O}$ and $[\text{Cu}_2(\text{mepirizole})_2(\text{C}_2\text{O}_4)(\text{NO}_3)_2(\text{H}_2\text{O})]_2[\text{Cu}_2(\text{mepirizole})_2(\text{C}_2\text{O}_4)(\text{NO}_3)_2]$. *Inorg. Chem.* **1989**, *28*, 3378–3386.
56. Osiry, H.; Cano, A.; Lemus-Santana, A.A.; Rodríguez, A.; Carbonio, R.E.; Reguera, E. Intercalation of organic molecules in 2D copper(II) nitroprusside: Intermolecular interactions and magnetic properties. *J. Solid State Chem.* **2015**, *230*, 374–380. [[CrossRef](#)]
57. Tang, J.; Costa, J.S.; Golobič, A.; Kozlevčar, B.; Robertazzi, A.; Vargiu, A.V.; Gamez, P.; Reedijk, J. Magnetic Coupling between Copper(II) Ions Mediated by Hydrogen-Bonded (Neutral) Water Molecules. *Inorg. Chem.* **2009**, *48*, 5473–5479. [[CrossRef](#)] [[PubMed](#)]